REFEREED PAPER

ADVANCED MODELLING OF HOMOGENOUS VOLATILE COMBUSTION THROUGH THE USE OF REDUCED CHEMICAL MECHANISMS

LAUBSCHER R

Sacks Circle, Bellville-South, 7530, Western Cape, South Africa

rynol@johnthompson.co.za

Abstract

The ability to harness the thermal energy from combustion is essential to existence on this planet. According to the International Energy Agency's 2013 Key World Energy Statistics report, 91.9% of the world energy is supplied by combustion processes. There is a broad range of applications of combustion; one of these is the combustion of coal and biomass such as sugarcane bagasse in watertube boilers. The current state-of-the-art in combustion modelling uses computational fluid dynamics, mixing based combustion models or chemical kinetics along with global and quasi-global chemical mechanisms to capture the complex processes. This approach is useful for designing stationary combustion processes, but is not ideally suited to capture time-dependant processes (quenching and ignition) and pollutant formation (SOx, NOx and unburned hydrocarbons). Combustion of solid fuels such as coal and biomass can be divided into the following sections: heating, evaporation, devolatilisation, volatile combustion and char oxidation. Combustion models are applied to solve the homogenous combustion of the volatile gases.

Current modelling techniques of combustion are comprised of two-step combustion models of the hydrocarbons, whereas the advance models use a chemical mechanism built up of multiple steps. The use of chemical mechanisms enables the engineer to model the NOx precursors (HCN, NH_3) and subsequent NOx reactions. These reactions can be used to optimise the combustion and secondary air system for NOx reduction and ensure less unburned hydrocarbon escapes the furnace (CH_4, C_3H_8). According to literature, 94% of the volatile gases released during devolatilisation is H_2, CH_4, CO_2 and CO (note this value is for a moisture free sample). Thus in this paper the combustion of these gases will be investigated.

This paper focuses on the use of different combustion models to predict gas mixture temperatures and species mass fractions, and then compares the current modelling approaches with an advanced approach. The results are then validated with experimental data.

Keywords: combustion, numerical modelling, chemical mechanisms, kinetics, emissions, CFD

Introduction

Combustion is a crucial part in various industries such as the production of engineering materials and power generation through the utilisation of the thermal energy released through the breaking of chemical bonds during rapid oxidation of fuels. The world realised that the fossil fuel resources are finite; major areas of research are shifted to energy production from

sustainable sources. One of these areas is biomass (including bagasse) combustion. This drive in biomass combustion research is due to the argument that the use of biomass in power generation is CO_2-neutral and therefore does not contribute to global warming (Bragato *et al*., 2011).

There are various types of biomass all with very different physical and chemical properties. Biomass is typically composed of cellulose, hemicellulose and lignin, as well as water, lipids, sugars, proteins and ash-forming elements. The combustion of biomass works much the same as fossil fuel combustion in that it has the same main chemical and physical processes taking place, namely sensible heating of the biomass particle, moisture evaporation, devolatilisation, homogeneous reactions of gaseous species with oxygen and with each other, char gasification and oxidation (Haseli *et al.,* 2011) (Haseli, van Oijen, & de Goey, 2011). Depending on various parameters such as particle size and density, surrounding gas temperature, and oxygen concentration, the above mentioned processes may occur sequentially or simultaneously (Haseli *et al.,* 2011) (Haseli, van Oijen, & de Goey, 2011). The main difference between biomass combustion and fossil fuel combustion is the mass fractions of the fixed carbon, volatiles, ash and moisture. Biomass has much higher mass fractions of volatiles and moisture than fossil fuels and thus has a higher percentage of energy being released due to gas phase reactions.

To investigate the accuracy of the combustion models a simple, axi-symmetric jet diffusion methane flame was chosen because extensive and accurate experimental measurements are available. The data was collected at Sandia National Labs. Methane combustion is very suited to investigation of bagasse volatile combustion; because within the complete combustion mechanism of methane the individual mechanisms for H_2, CH_4, CO_2 and CO are found and, as mentioned, 94% of volatile gases are comprised of these constituents (Zanzi *et al*., 1995) (Zanzi, Bjornbom, & Sjostrom, 1995). Thus the various modelling parameters for bagasse volatile combustion can be investigated and validated with the Sandia experimental setup. This type of investigative approach was also undertaken by Scharler *et al.* (2003) where the authors investigated modifying the Eddy dissipation model/Finite-Rate-Kinetics model for boiler grate furnaces, by tuning the model constants.

The Eddy dissipation model combustion model simulation uses a reduced chemical mechanism of 41 reactions and 16 species (ANSYS, 2009), whereas the Eddy dissipation model/Finite-rate-kinetics uses a two-step methane combustion reaction (Westbrook and Dryer Two-step mechanism) with five species (Wang e*t al.,* 2012). Therefore the study will investigate the performance of these two approaches for modelling bagasse homogenous combustion.

Literature study

The current state-of-the-art in combustion modelling is the use of the Eddy-dissipation model along with global reaction kinetics (EDM/FRK) and using empirical correlations to determine the reaction rates of the chemical reactions and post processing correlations to determine the NO_x formation. The popularity of the EDM/FRK models comes from their low computational costs, especially for industrial applications. However, the empirical constants are not universally valid and need to be adapted depending on the application (Shienejadhesar *et al*., 2014). Further using more than two reactions with the EDM/FRK will produce incorrect solutions. The reason for this is that the multi-step chemical mechanisms are based on Arrhenius rates, which differ for each reaction. In the EDM/FRK model, reaction has a single

rate and therefore the model can only be used for single-step and two-step reactions. To incorporate multi-step chemically kinetic mechanisms in turbulent flows, the Eddy dissipation concept (EDC) model is much more suited because each chemical reaction is treated individually. Thus in this section the theory behind these two combustion approaches will be presented along with the standard modelling equations for mass, species, momentum, energy, kinetic energy and dissipation rate.

Below are the continuity, species, momentum and energy equations with their additional relations presented.

Continuity: $\frac{\partial}{\partial x}(\rho u_x) + \frac{\partial}{\partial y}(\rho u_y) + \frac{\partial}{\partial z}(\rho u_z) = S_m$

Ideal gas law: $p = \rho \frac{R}{M} T$

Species:

$$\rho\left(u_x \frac{\partial Y_k}{\partial x} + u_y \frac{\partial Y_k}{\partial y} + u_z \frac{\partial Y_k}{\partial z}\right) + \frac{\partial}{\partial x}(\rho Y_k V_{kx}) + \frac{\partial}{\partial y}(\rho Y_k V_{ky}) + \frac{\partial}{\partial z}(\rho Y_k V_{kz}) = \omega_k + S_k$$

$$V_{kx} = -\frac{D}{Y_k}\frac{\partial Y_k}{\partial x}, V_{ky} = -\frac{D}{Y_k}\frac{\partial Y_k}{\partial y}, V_{kz} = -\frac{D}{Y_k}\frac{\partial Y_k}{\partial z}$$

Momentum equations (x,y and z directions):

$$\rho\left(u_x \frac{\partial u_x}{\partial x} + u_y \frac{\partial u_x}{\partial y} + u_z \frac{\partial u_x}{\partial z}\right) = -\frac{\partial p}{\partial x} + \left(\frac{\partial \tau_{xx}}{\partial x} + \frac{\partial \tau_{yx}}{\partial y} + \frac{\partial \tau_{zx}}{\partial z}\right) + B_x$$

$$\rho\left(u_x \frac{\partial u_y}{\partial x} + u_y \frac{\partial u_y}{\partial y} + u_z \frac{\partial u_y}{\partial z}\right) = -\frac{\partial p}{\partial y} + \left(\frac{\partial \tau_{xy}}{\partial x} + \frac{\partial \tau_{yy}}{\partial y} + \frac{\partial \tau_{zy}}{\partial z}\right) + B_y$$

$$\rho\left(u_x \frac{\partial u_z}{\partial x} + u_y \frac{\partial u_z}{\partial y} + u_z \frac{\partial u_z}{\partial z}\right) = -\frac{\partial p}{\partial z} + \left(\frac{\partial \tau_{xz}}{\partial x} + \frac{\partial \tau_{yz}}{\partial y} + \frac{\partial \tau_{zz}}{\partial z}\right) + B_z$$

Where the components of the stress tensor for Newtonian fluids in rectangular coordinates in equations above is given by:

$$\tau_{xx} = \mu\left[2\frac{\partial u_x}{\partial x} - \frac{2}{3}(\nabla \cdot \boldsymbol{u})\right] \quad \tau_{yy} = \mu\left[2\frac{\partial u_y}{\partial y} - \frac{2}{3}(\nabla \cdot \boldsymbol{u})\right] \quad \tau_{zz} = \mu\left[2\frac{\partial u_z}{\partial z} - \frac{2}{3}(\nabla \cdot \boldsymbol{u})\right]$$

$$\tau_{xy} = \mu\left[2\frac{\partial u_x}{\partial y} - \frac{\partial u_y}{\partial x}\right] \qquad \tau_{xz} = \mu\left[2\frac{\partial u_x}{\partial z} - \frac{\partial u_z}{\partial x}\right] \qquad \tau_{zy} = \mu\left[2\frac{\partial u_y}{\partial z} - \frac{\partial u_z}{\partial y}\right]$$

Energy equation:

$$\rho\left(u_x \frac{\partial h_t}{\partial x} + u_y \frac{\partial h_t}{\partial y} + u_z \frac{\partial h_t}{\partial z}\right) - \left(u_x \frac{\partial p}{\partial x} + u_y \frac{\partial p}{\partial y} + u_z \frac{\partial p}{\partial z}\right) = k\left(\frac{\partial^2 T}{\partial x^2} + \frac{\partial^2 T}{\partial y^2} + \frac{\partial^2 T}{\partial z^2}\right) -$$
$$\sum_{k=1}^{N} \omega_k \Delta h_{f,k}^0 - S_{rad} - \left[\frac{\partial}{\partial x}(\rho \sum_{k=1}^{N} h_k Y_k V_{kx}) + \frac{\partial}{\partial y}\left(\rho \sum_{k=1}^{N} h_k Y_k V_{ky}\right) +\right.$$
$$\left.\frac{\partial}{\partial z}(\rho \sum_{k=1}^{N} h_k Y_k V_{kz})\right] + \mu\left\{2\left[\frac{\partial u_x}{\partial x}^2 + \frac{\partial u_y}{\partial y}^2 + \frac{\partial u_z}{\partial z}^2\right] + \left[\frac{\partial u_y}{\partial x} + \frac{\partial u_x}{\partial y}\right]^2 + \left[\frac{\partial u_z}{\partial y} + \frac{\partial u_y}{\partial z}\right]^2 +\right.$$
$$\left.\left[\frac{\partial u_z}{\partial x} + \frac{\partial u_x}{\partial z}\right]^2 - \frac{2}{3}\left[\frac{\partial u_x}{\partial x} + \frac{\partial u_y}{\partial y} + \frac{\partial u_z}{\partial z}\right]^2\right\} + \rho \sum_{k=1}^{N} Y_k\left(f_{kx} V_{kx} + f_{ky} V_{ky} + f_{kz} V_{kz}\right)$$

Turbulence is characterised by random fluctuations of all the fluid properties through time and space at sufficiently high Reynolds numbers, depending on the geometry of the fluid field (Poinsot and Veynante, 2005). Mathematically any property in the flow field f is usually split into a mean value $\bar{f}$ and a fluctuating component f'. Thus velocity, species mass fraction, total enthalpy, pressure and stresses tensor variables in the above equations must be substituted by the mean and fluctuating property for turbulent flow (the derivation is quite tedious and will not be shown). This procedure is called the Reynolds time-averaging. Reynolds averaging introduces three new terms namely Reynolds turbulent stresses ($-\bar{\rho}\overline{u_i'u_j'}$) in the momentum equations, turbulent species flux ($\overline{u_i'Y_k'}$) and the enthalpy turbulent flux ($\overline{\rho u_i'h'}$). To be able to perform turbulent calculations to evaluate these new flow quantities is referred to as the turbulent 'closure' problem (Kays and Crawford, 2005). These extra three flow quantities are solved using a turbulence model. The turbulence model used in this paper is the $k-\varepsilon$ realisable turbulence model. The term 'realisable' means that the model satisfies certain mathematical constraints on the Reynolds stresses, consistent with the physics of turbulent flows (ANSYS, 2009). The main differences between the standard $k-\varepsilon$ model and the realizable model is: in the new model dissipation rate equation is based on the dynamic equation for fluctuating vorticity (Shih, 1995) and the new eddy viscosity formulation ensures realisability and contains the effect of mean rotation and turbulent stresses (Shih, 1995). The eddy dissipation equation's production term is similar to the spectral energy transfer concept and is believed to capture turbulent vortex stretching and dissipation terms more accurately according to (Shih, 1995). The model equations are according to (Shih, 1995);

$$\frac{\partial}{\partial x_j}(\rho k u_j) = \frac{\partial}{\partial x_j}\left(\left[\mu + \frac{\mu_t}{\sigma_k}\right]\frac{\partial k}{\partial x_j}\right) - \bar{\rho}\overline{u_i'u_j'}\frac{\partial \overline{u_i}}{\partial x_j} + G_b - \rho\varepsilon$$

$$\frac{\partial}{\partial x_j}(\rho \varepsilon u_j) = \frac{\partial}{\partial x_j}\left(\left[\mu + \frac{\mu_t}{\sigma_\varepsilon}\right]\frac{\partial \varepsilon}{\partial x_j}\right) + \rho C_1 S_\varepsilon - \rho C_2 \frac{\varepsilon^2}{k+\sqrt{\nu\varepsilon}} + C_{1\varepsilon}\frac{\varepsilon}{k}C_{3\varepsilon}G_b$$

$$C_1 = max\left[0.43, \frac{\eta}{\eta+5}\right], \eta = S\frac{k}{\varepsilon} \text{ and } S = \sqrt{2S_{ij}S_{ij}}$$

The model constants for the $k-\varepsilon$ realisable turbulence model is:

$$C_{1\varepsilon} = 1.44, C_2 = 1.9, \sigma_k = 1.0\,, \sigma_\varepsilon = 1.2$$

It was found that realisable $k-\varepsilon$ model predicted more accurate results for flows without pressure gradients, rotating homogeneous flows, boundary-free shear flows and backward facing step flow than the standard turbulence model. It also enhances numerical stability in turbulent flow calculations (Shih, 1995). Therefore because of the spreading jet anomaly observed for the Sandia jet diffusion flame this turbulence model predicts the flow field more accurate than other two-equation turbulence models.

Next the two combustion modelling approaches will be stated. The EDM/FRK approach relates the rate of combustion to the rate of dissipation of eddies and expresses the rate of reaction by the mean concentration of the reacting species, turbulent kinetic energy and the rate of dissipation of this energy (Magnussen and Hjertager, 1976). It also compares this rate with the rate of the chemical reactions and uses the limiting/minimum value for the reaction rate in the energy and species transport equations.

$$\omega_{k,j} = \nu'_{k,j} M_{w,k} A\rho \; min\left(\frac{Y_R}{\nu'_{R,j} M_{w,r}}\right)$$

$$\omega_{k,j} = \nu'_{k,j} M_{w,k} AB\rho \frac{\varepsilon}{k} \frac{\sum_P Y_P}{\sum_N^i \nu''_{i,j} M_{w,j}}$$

where *A* and *B* are the constants which were experimentally determined by Magnussen and Hjertager (1976), and are 4 and 0.5 respectively. If the minimum of these two equations is less than the value calculated by:

$$\omega_{k,j} = M_k \sum_{j=1}^{Z} \left(\nu''_j - \nu'_j\right)\left[K_{fj} \prod_{k=1}^{N} [X_k]^{\nu' kj} - K_{rj} \prod_{k=1}^{N} [X_k]^{\nu'' kj}\right]$$

The reaction rate is said to be mixing limited, therefore the chemical reaction is limited by the rate at which reactants and oxidizer mix. If the chemical reaction rate is less the reaction is said to be kinetically limited. The main disadvantage is that the model cannot account for strong coupling between turbulence and multi-step chemistry, and thus is insufficient to capture NOx production, and extinction of combustion. Another disadvantage is the fact that the empirical parameter *A* is not universally valid and depends on application.

Chemical reactions take place when reactants are mixed at a molecular scale at sufficiently high temperature. In turbulent flow the reaction is highly dependent on the molecular mixing rate. The micro scale processes which are required for molecular mixing and turbulent energy dissipation are very sparse in time and space and these processes are confined to isolated regions whose entire volume is only a small fraction of the fluid volume. The micro scale regions in turn are comprised of fine structures. These structures have the same characteristic dimensions as the Kolmogorov micro scales. The fine structures are responsible for the dissipation of turbulence into heat. Within these structures we can thus assume that the reactants will be molecularly mixed due to the small length and velocity scales. The EDC uses these fine structures as small, well mixed chemical reactors to combust the chemical constituents of the gas in the fluid volume. The derivation of the EDC variables is quite tedious and will not be presented in this paper. The model uses the energy cascade to determine the mass fraction that fine structures occupy of the fluid volume and the mass transfer rate into the fine structures. The rate of molecular mixing is determined by the rate of mass transfer between the surrounding fluid and the fine structures. Mean transfer between the fine structures and the rest of the fluid for a certain species k can be expressed as:

$$\omega_k = \frac{\rho \dot{m}^* \gamma^*}{1-\gamma^*} (\bar{Y}_k - Y_k^*)$$

where Y_k^* is the fine structures mass fraction after reacting over the mixing or chemical time scales (depending which is the limiting process), and $\bar{Y}_k$ mean species mass fraction in the surrounding fluid. According to (ANSYS, 2009) the combustion at the fine structures is assumed to occur as a constant pressure reactor, with initial conditions taken as the current species fraction and temperature in the control volume. As mentioned the reactions occur over the limiting time scale and are governed by the Arrhenius rates and are integrated numerically. Thus the ordinary differential equation which produces or destroys species k is expressed as:

$$\frac{dY_k^*}{d\tau^*} = \omega_k + \dot{m}^*(Y^0 - Y^*)$$

This model therefore enables the engineer to model combustion and turbulence chemistry on a more fundamentally correct approach, which does not need tuning. Now that the governing

theory was briefly presented, in the next section the experimental and numerical setup will be discussed.

Numerical modelling and experimental setup

Sandia National Labs has performed extensive tests on methane flames at different velocities. A set of flames ranging from laminar (denoted Flame A), transitional flow (Flame B), fully turbulent (Flame D) and near extinguished (Flame F) were tested. The following scalars are measured: T, N_2, O_2, CH_4, CO_2, H_2O, H_2, OH, NO and CO. Due to the high induced turbulence from the air flow through a boiler grate and secondary air nozzles lead to turbulent combustion within boiler furnaces. Therefore only Flame D (fully turbulent combustion) was simulated and investigated with the two combustion models. The secondary air injection velocity in a boiler furnace is between 20-90 m/s and the Flame D velocity is 49.6 m/s. Therefore the combustion behaviour will be similar to combustion in a furnace as mentioned.

The burner, consisting of a main round jet and a concentric pilot, was placed in a wind tunnel. The main jet consists of methane and air. The pilot is a lean fuel/air mixture which is used for flame stabilisation (Shienejadhesar *et al.*, 2014). See Figure 1 for the geometry and applied boundary conditions. See Table 1 for burner dimensions.

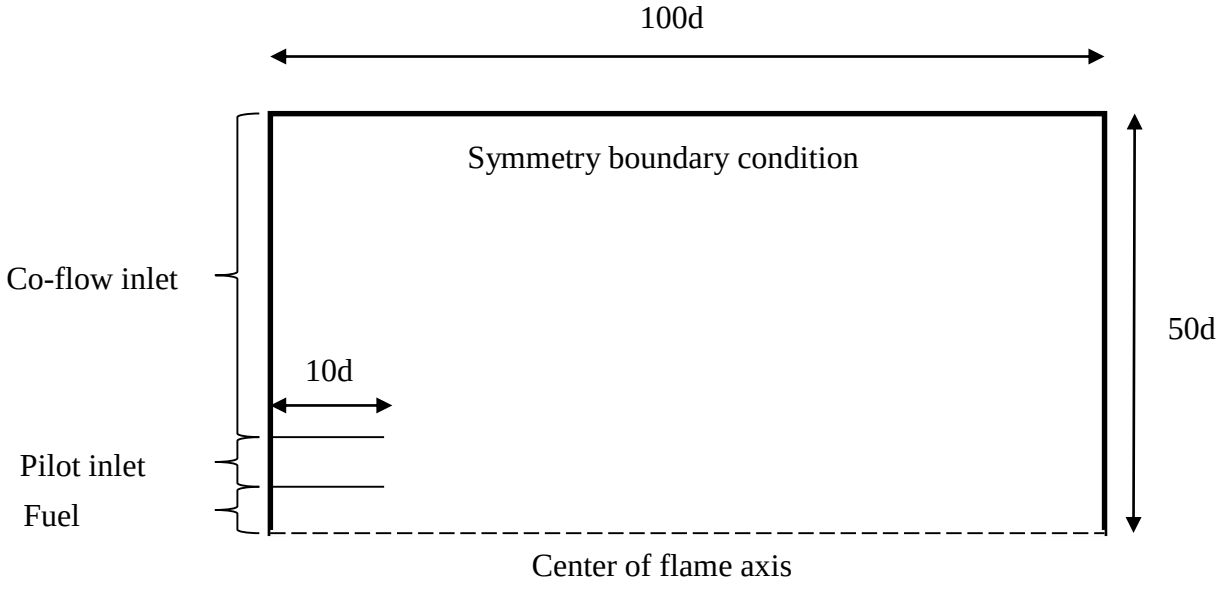

Figure 1. Burner geometry and boundary designation.

Table 1. Burner dimensions.

Main jet inner diameter, d	7.2 mm
Pilot annulus inner diameter	7.7 mm (wall thickness = 0.25 mm)
Pilot annulus outer diameter	18.2 mm
Burner outer wall diameter	18.9 mm (wall thickness = 0.35 mm)
Wind tunnel exit	300 mm x 300 mm

The burner was modelled as a 2D-axisymmetric domain due to the symmetry of the burner as seen in Figure 1. The governing equations as shown in the Literature study were solved using Fluent. The discrete ordinances radiation together with Weighted-Sum-of-Gray-Gases method was used to solve the radiative heat transfer equation. The In-Situ Adaptive Tabulation (ISAT) method was used to solve the chemistry and to speed up the solution time. The models' convergence criteria were set to 0.001 for all fluid variables except DO-intensity and energy which was set to 1E-6. Table 2 shows the boundary conditions used in the simulations.

Table 2. Boundary condition for CFD simulations.

Designation	Boundary condition type	Value
Center line axis of flame	Axis	-
Co-flow inlet	Velocity inlet	Velocity magnitude = 0.9 m/s Temperature = 291 K Internal emissivity = 1 Y_{O2} = 0.233
Jet inlet	Velocity inlet	Velocity magnitude = 49.6 m/s Temperature = 294 K Internal emissivity = 1 Y_{O2} = 0.19664 Y_{CH4} = 0.15607
Jet wall	Wall	Heat flux = 0 W/m^2 Opaque surface
Outlet	Pressure outlet	Backflow temperature = 291K Backflow Y_{O2} = 0.233
Pilot	Velocity inlet	Velocity magnitude = 11.4 m/s Temperature = 1908 K Internal emissivity = 1 Y_{O2} = 0.056 Y_{CO2} = 0.11 Y_{H2O} = 0.092
Pilot wall	Wall	Heat flux = 0 W/m^2

In the next section the results for the EDM/FRK with two-step mechanism (Wang *et al*., 2012) and EDC with 41 step reduced mechanism (ANSYS, 2009) CFD combustion simulations will be presented and compared to experimental data, to determine the accuracy and shortcomings of the two models.

Results and Discussion

Data from Sandia was taken on the center line axis of the flame at axial distances of 75, 150, 300, 450, 600 and 750 mm from the jet nozzle inlet of the domain. The results analysed are the temperature profile and CO, CO_2, O_2, CH_4 and H_2O mass fractions. The results of these scalars can be seen in Figures 2-5, where the X-axis is the normalised distance.

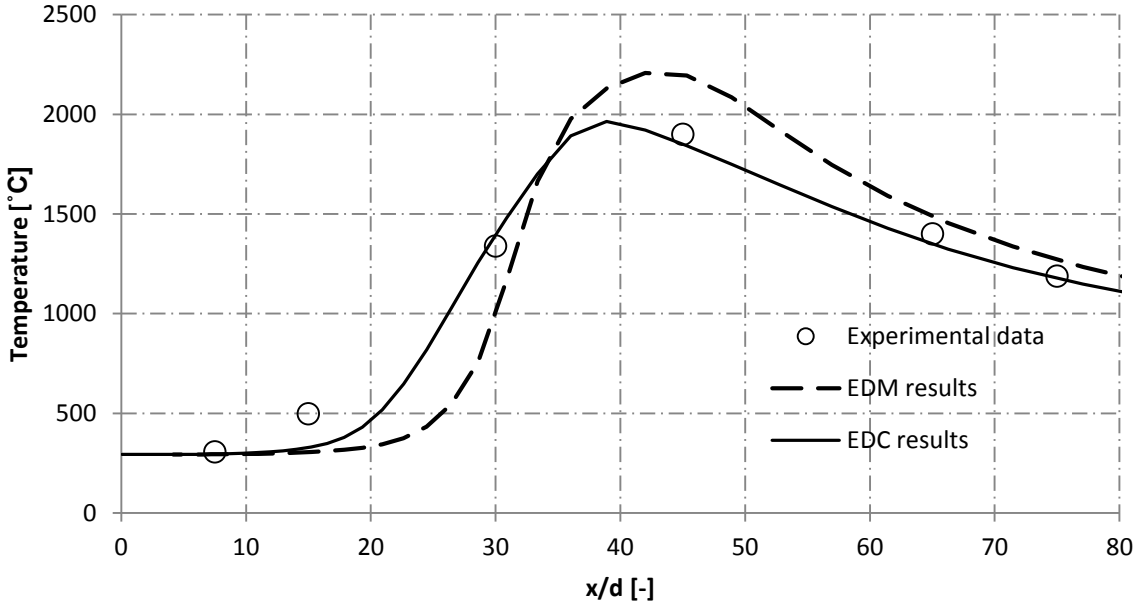

Figure 2. Gas temperature vs. normalized axial distance on center line of flame.

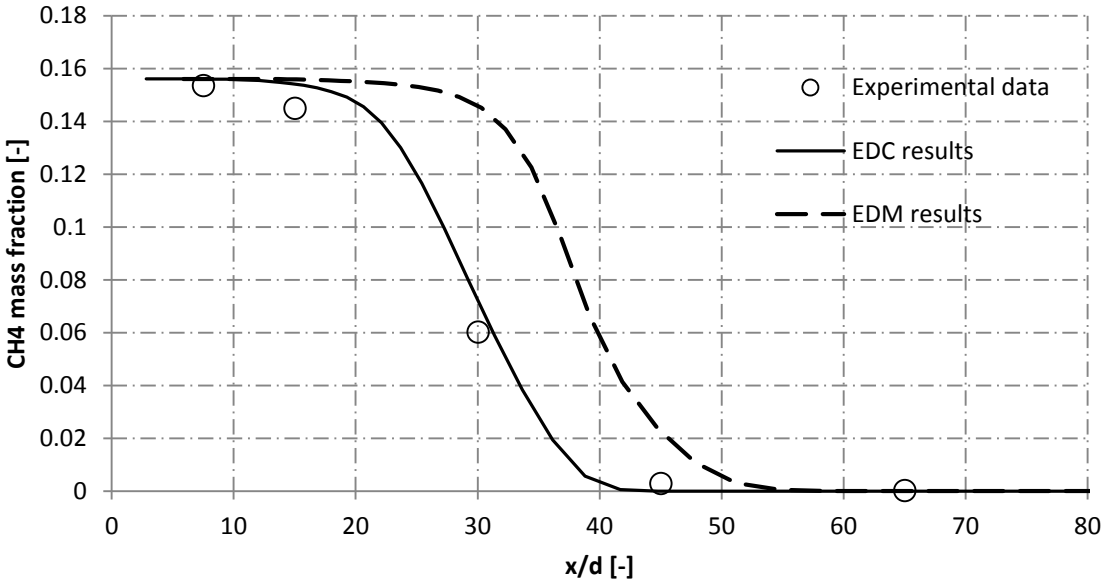

Figure 3. CH_4 mass fraction vs. normalised axial distance on center line of flame.

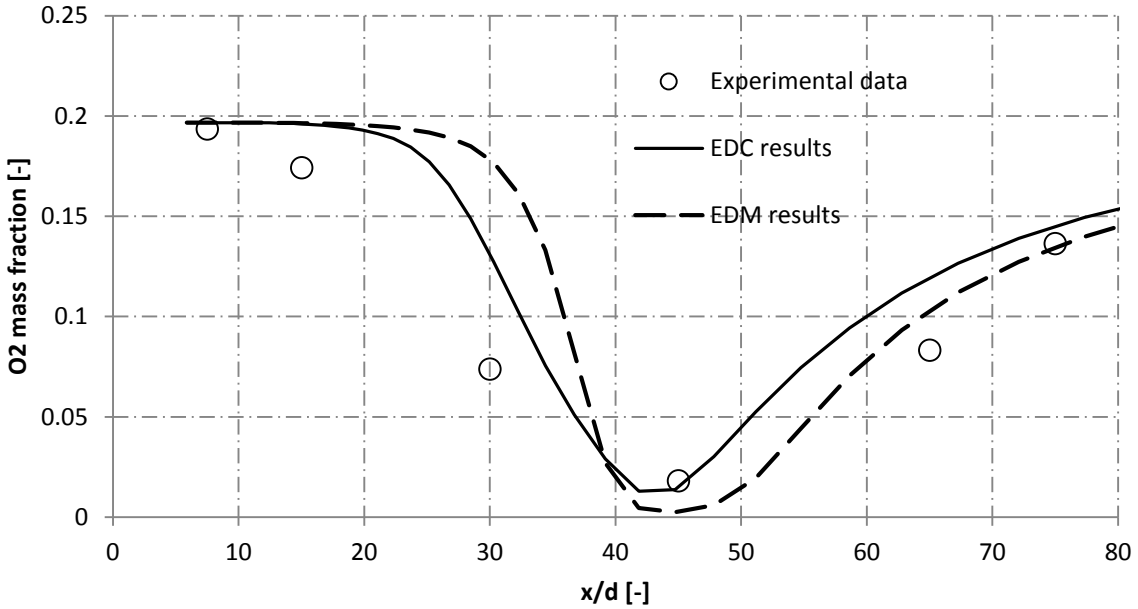

Figure 4. O_2 mass fraction vs. normalized axial distance on centre line of flame.

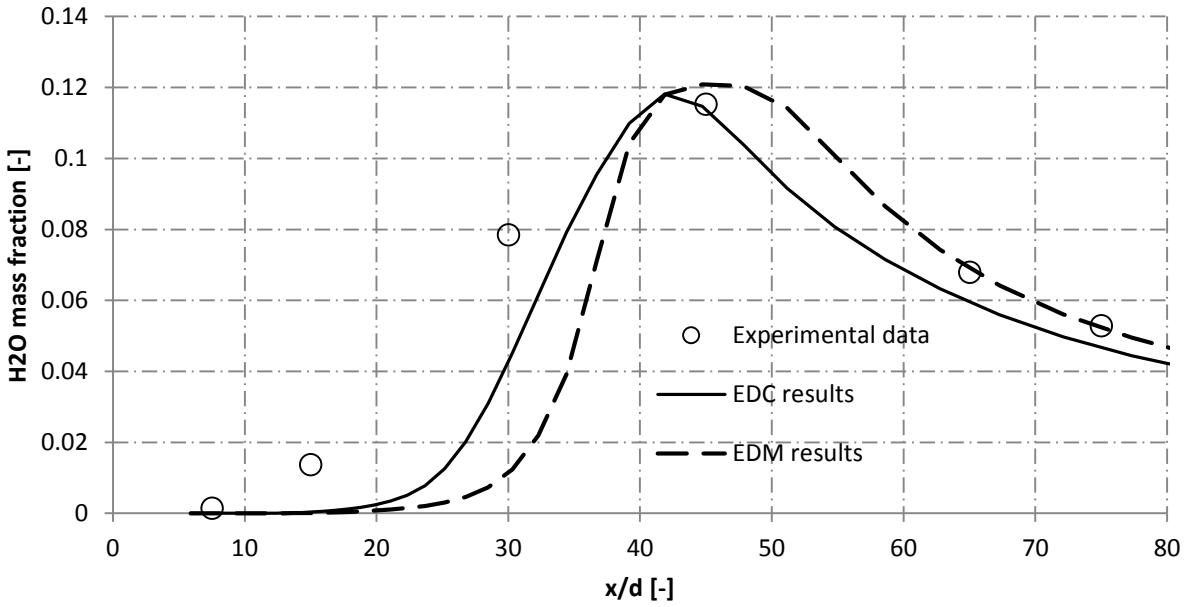

Figure 5. H_2O mass fraction vs. normalised axial distance on centre line of flame.

From Figures 2-5 it can be clearly seen that the EDC with the 41 reactions predicts the temperature and mass fraction more accurately than the current state-of-the-art EDM/FRK with 2-step reaction model. The major increase in accuracy is seen in the prediction of the temperature, CO and CO_2 mass fractions. The combustion reaction rate predicted by the EDM/FRK model is mixing limited and has a max reaction rate of 0.886 kgmol/m^3-s and the EDC model predicts a max net reaction rate for CO of 0.6125 kgmol/m^3-s. Therefore the EDC produces the CO much slower than the EDM/FRK model and the reaction rate at which CO is consumed is 0.39 kgmol/m^3-s for the EDC and 0.98 kgmol/m^3-s for the EDM/FRK model. Therefore the EDM/FRK over predicts the CO_2 production rate and thus and under predicts the CO mass fraction. This also yields over-prediction of the gas temperature as seen in Figure 2, due to rapid release of the energy due to CO_2 formation.

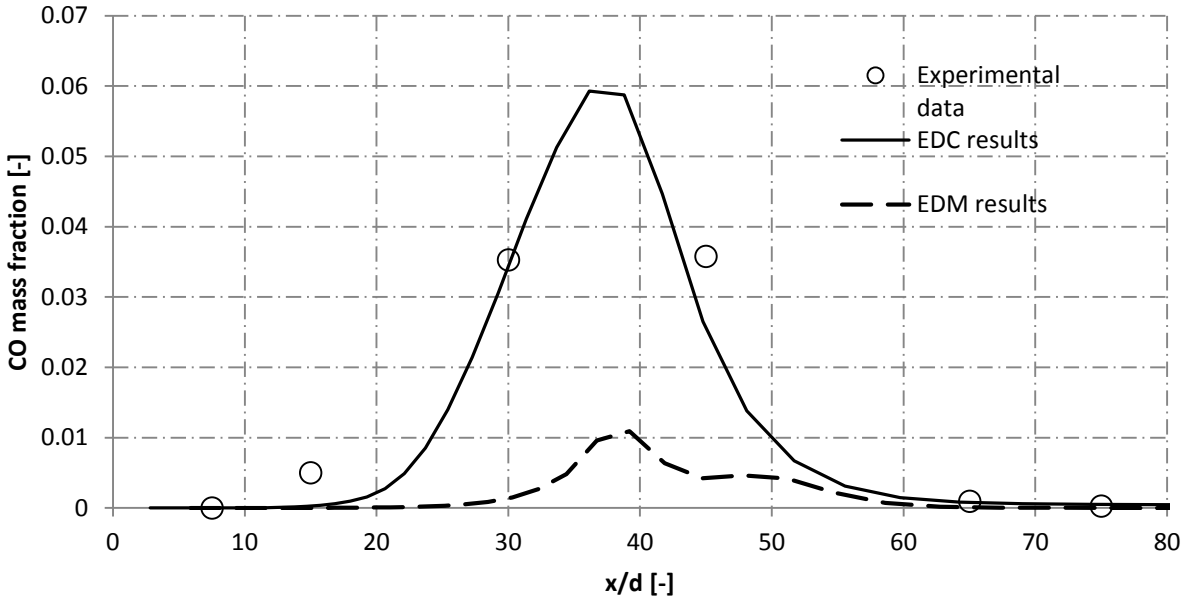

Figure 6. CO mass fraction vs. normalised axial distance on centre line of flame.

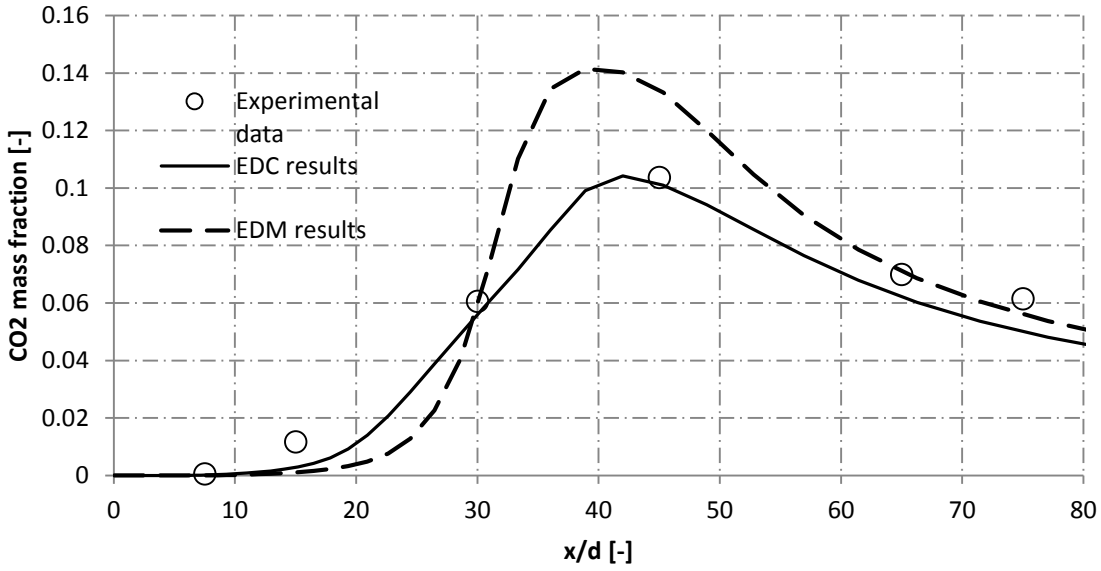

Figure 7. CO_2 mass fraction vs. normalised axial distance on centre line of flame.

Because the EDM/FRK uses the large energy bearing eddies' lifetime to determine the mixing rate, but in reality, as mentioned, molecular mixing required for chemical reactions occurs in the fine structures which have the same scale as the Kolmogorov scales. Therefore the lifetime of the eddies (small/fine scales) which causes molecular mixing is much shorter than for the large eddies. Therefore Magnussen (1981), developer of EDM/FRK, used an *A* constant (manually tuned parameter to curve fit data) to try and capture small-scale mixing by multiplying the eddy break-up rate (inverse of eddy lifetime) by it. However, depending on the flow fields (turbulent Reynolds number) and the chemical species the rate of actual mixing changes rapidly, the value of 4 is therefore only applicable to the experimental setup Magnussen used. As seen in Figures 6 and 7, the reaction rate of CO with O_2 should be decreased and therefore a lower *A* constant must be used. The reason for this is that the ratio between large eddies and small scale eddies differ for the Sandia experimental setup to the

original tests performed by Magnussen. Now that the EDC combustion is shown to be superior to the EDM/FRK model, in the next section the EDC model with a newly formulated multi-step chemical mechanism was implemented in an industrial sized boiler model.

Boiler application of eddy dissipation concept

In this section an industrial boiler was modelled in ANSYS Fluent, solving the same equations as presented in the Literature study. The EDC combustion model was used and solved using direct integration. The gas-phase reaction mechanism used was the Jones-Lindstedt 4-step combustion mechanism for alkane hydrocarbons up to butane. In this model a pseudo-biomass volatile was used to represent the volatiles driving off during devolatilisation. The composition and formation enthalpy of the pseudo volatile is determined from the proximate and ultimate analysis of the bagasse data. The chemical mechanism can be seen below (Chungen *et al*., (2010):

$$C_X H_y O_z N_q \equiv aCH_4 + bC_3H_8 + cH_2 + dCO + eHCN + fNH_3 + gCO_2$$

$$CH_4 + 0.5O_2 \rightarrow CO + 2H_2$$
$$CH_4 + H_2O \rightarrow CO + 3H_2$$
$$H_2 + 0.5O_2 \rightarrow H_2O$$
$$H_2O \rightarrow H_2 + 0.5O_2$$
$$CO + H_2O \leftrightarrow CO_2 + H_2$$
$$C_3H_8 + 1.5O_2 \rightarrow 3CO + 4H_2$$
$$C_3H_8 + 3H_2O \rightarrow 3CO + 7H_2$$

Therefore the model assumes the pseudo molecule to be formed during devolatilisation. The EDC combustion then takes over and solves the homogenous combustion of this molecule and the subsequent reaction as seen above. *HCN* and *NH3* are included for subsequent NOx simulations, seeing as they are major precursors to NOx formation.

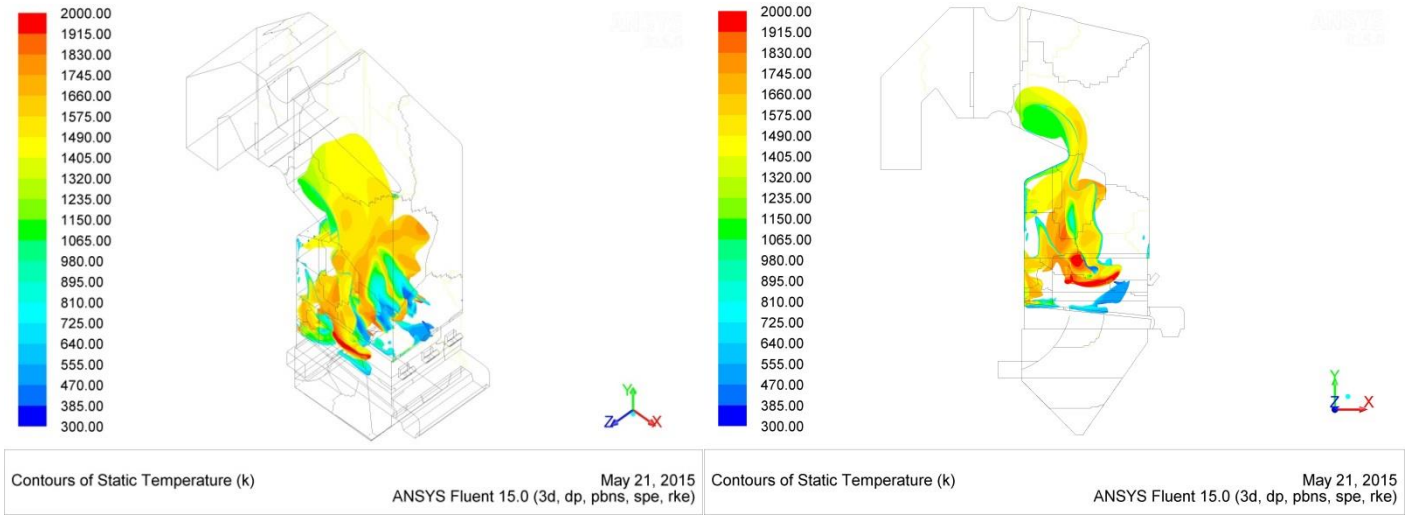

Figure 8. Flame temperature profile for eddy dissipation concept combustion model.

The figures below show the contour plots flame temperature profile for the EDC and

EDM/FRK. It must be noted that the superheater was not modelled; therefore the actual flame temperature will be slightly lower and the flame slightly smaller.

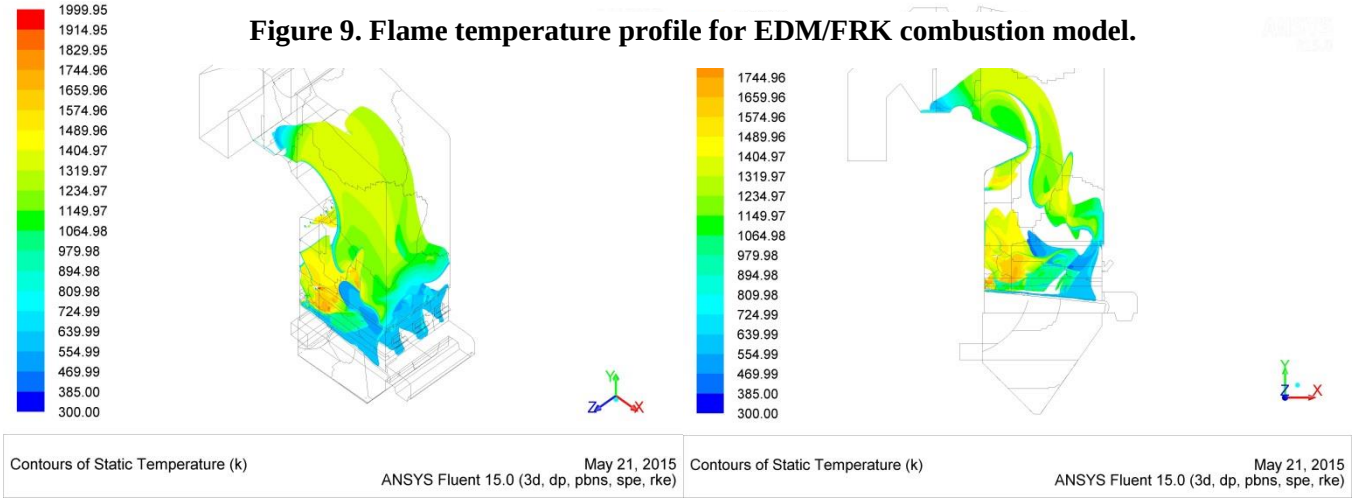

Figure 9. Flame temperature profile for EDM/FRK combustion model.

Figure 8. Flame temperature profile for EDC combustion model.

The EDM/FRK model as seen in Figure 9 has a tuned Magnussen constant (*A*) to produce results similar to site measurements. The model still predicted a larger flame (validated with visual observations) and higher CO (measured on site), from Figure 8 it is seen that the EDC predicts a smaller flame which has lower CO. The modelling of bagasse combustion

Conclusion and future work

The following conclusions can be made:

- In this paper it was shown that the advance EDC combustion model is more theoretically correct and accurate to the current-state-of-the-art EDM/FRK combustion model. In that the EDM/FRK has a tuning parameter which must be adjusted for each application whereas the EDC does not have to be tuned and is fundamentally correct for turbulent combustion analysis.
- The Sandia Flame D was successfully modelled and results were close to the experimental data points.
- The EDC is able to solve multi-step chemistry required for advance combustion analysis such as NOx formation whereas the EDM/FRK is unable to produce accurate results.

Future work:

- Validate EDC model with site data and include superheater into EDC CFD model to account for additional heat extraction and the determine effect it has on chemical species formation.
- Model NOx formation chemical reactions.

REFERENCES

ANSYS (2009). ANSYS Advanced Combustion Modeling Course. ANSYS Inc.

Bragato M, Kulbhushan J, JB C, Tenorio J and Levendis Y (2011). Combustion of coal, bagasse and blends thereof. Part II: Speciation of PAH emissions. *Fuel* 51-58.

Chungen Y, Kaer S, Rosendahl L and Hvid S (2010). Co-firing straw with coal in a swirl-stabilized dual-feed burner: Modelling and experimental validation. *Bioresource Technology* 101: 4169-4178.

Haseli Y, van Oijen J and de Goey L (2011). A detailed one-dimensional model of combustion of a woody biomass particle. *Bioresource Technology* 131: 9772-9782.

Kays W and Crawford M (2005). *Convective Heat and Mass Transfer*. McGraw Hill.

Magnussen B (1981). On structure of turbulence and a generalized eddy dissipation concept for chemical reaction in turbulent flow. *American Institute of Aeronautics and Astronautics* .

Magnussen B and Hjertager B (1976). On mathematical modelling of turbulent combustion with special emphasis on soot formation and combustion. 16th Symposium on Combustion .

Poinsot T and Veynante D (2005). *Theoretical and Numerical Combustion*. 2nd edition. Edwards.

Scharler R, Fleckl T and Obernberger I (2003). Modification of a Magnussen Constant of the Eddy Dissipation Model for biomass grate furnaces by means of hot gas in-situ FT-IR absorption spectroscopy. *Progress in Computational Fluid Dynamics* 3: 102-111.

Shienejadhesar A, Mehrabia R, Scharler R and Goldin G (2014). Development of a gas phase combustion model suitable for low and high temperature turbulence conditions. *Fuel* 177-187.

Shih T (1995). A new k-epsilon eddy viscosity model for high Reynolds number turbulent flows. *Computer Fluids* 227-238.

Wang L, Zhaohui L, Chen S and Zheng C (2012). Comparison of different global combustion mechanisms under hot and diluted oxidation conditions. *Combustion Science and Technology* 184(2): 259-276.

Zanzi R, Bjornbom E and Sjostrom K (1995). Rapid pyrolysis of bagasse at high temperature. Proceedings of Third Asia-Pacific International Symposium on Combustion and Energy Utilization, Hong Kong. pp 211-215.